FVPM simulation of scratching induced by a spherical indenter

Charly Euzenat, Sylvain Lavernhe, Christophe Tournier

FVPM simulation of scratching induced by a spherical indenter

Charly Euzenat[a,*], Sylvain Lavernhe[a], Christophe Tournier[a]

[a] *LURPA, ENS Paris-Saclay, Univ. Paris-Sud, Université Paris-Saclay, 94235 Cachan, France.*

Abstract

This article presents a single particle scratching simulation using the Finite Volume Particle Method (*FVPM*). *FVPM* is a variant of the well-known Smooth Particles Hydrodynamics method (SPH) which is locally conservative and consistent, what's more it features advantages of mesh-free methods for handling moving interfaces and multi-scale interpolation. The test material is represented by overlapping particles and data exchanges occur through the interfaces. The indenter is modeled as a rigid sphere whose path is a straight horizontal line. The resulting surface topography as well as constraints and scratching efforts have been numerically studied. The *FVPM* simulation code assessed in this article has been found suitable for the scratching simulation based on a comparison with other results from the literature. The presented results suggest the possibility to simulate more complex surface finishing operations. Manufacturing processes based on abrasion material removal, such as the grinding process, will be considered in the future.

Keywords: Scratching, *FVPM*, Grinding, Multi-scale Modeling.

1. Introduction

The performances of high added value parts are strongly linked with the ability to master the manufacturing process at all involved steps. In industry, finishing operations based on abrasion material removal play a major role in ensuring functional requirements and remain mandatory to improve surface characteristics after machining whether the surface is designed to provide optical, friction, or aerodynamic functions. The abrasion process is characterized by complex interactions between the abrasive tool and the machined surface in order to remove and repel matter. These interactions are generated by the path of sharp particles, inducing grooves over the surface [1]. The global geometric shape as well as the local texture of the surface are affected by the process which, in turn, may influence the overall quality and limits the service lifespan of mechanical components. In these regards, manufacturers meet their requirements relying on empirical rules combined with an experienced based know-how. The contributions of models and simulation algorithms are not limited to improving the manufacturing process but also allow a better understanding of the abrasion mechanism itself.

The modeling of material removal mechanism has been investigated through several techniques. The chip thickness, the induced grinding force along with the thermal effects models have been developed. A review of these grinding models has been proposed by [2] and a multi-scale review of the experimental and simulation approaches has been proposed by [3]. Several ways of defects have been identified by [4]. Three hypotheses have been made to describe the removal mechanisms. The flow hypothesis and the abrasion hypothesis are mechanical interactions inducing high local strain and stress to remove and repel matter. The mechanical defects induced by the abrasive particles fall into four main categories :

- Microploughing
- Microfatigue
- Microcutting
- Microcracking

The plastic deformations encountered by the specimen, repels the material at the sides of the grooves and results in microploughing. The pile up model developed in [5] accounts for these plastic deformations in microploughing. Depending on the material characteristics, the interactions may although generate chips and cut the specimen instead of creating bulges. Microfatigue occurs when several grains paths are located in the same area until the material fails. Brittle materials like ceramics are more subjected to microcracking as a result of high stress induced by abrasive particles.

From a macroscopic and empirical point of view, several models exist in order to predict the surface obtained following a finishing process. One of the most common to induce the removal rate is the Preston model [6] (Eq. 1).

$$\frac{dz}{dt} = K_p.P.V \tag{1}$$

*Corresponding author. Tel.: +33(0) 1 47 40 27 58.
E-mail address: charly.euzenat@ens-paris-saclay.fr (Charly Euzenat).

This equation reflects the fact that the removal rate is related to both the contact pressure P and the relative velocity V. The Preston coefficient K_p is the equivalent for the efficiency of the abrasive tool against process parameters. Several other laws derived from the Preston model have been proposed to improve the prediction relevance.

$$\frac{dz}{dt} = K_p.P^{\alpha}.V^{\beta} \tag{2}$$

Klocke [4] has developed a general-purpose model for abrasion (Eq. 2) with two additional degrees of freedom in the equation. This model requires more involved identification procedure yet offers a wider range of possibilities while modeling various tool-workpiece pairs. Whatever the shape of the equations, the laws identified above are mainly used as a description of the interactions but are not yet implemented in simulations on their own.

Applying the concept of continuum mechanics to abrasion is under high investigation in the literature, especially allowed by recent development of computing capabilities. Still, the simulation of a complete abrasion process is out of reach within reasonable computational time, this is why test cases involving a single abrasive grain are often preferred to evaluate numerical methods. The scratching test procedure is used to characterize a material under the path of a spherical indenter and can be considered as the basic interaction involved during abrasion. This elementary damage procedure has been previously chosen by [7] for the validation of SPH simulation code. Single grain scratching and impact have been successfully simulated using both FEM and meshless numerical methods [8, 9].

2. Theory

During a simulated scratching, the material cohesion and behavior inside the specimen is numerically emulated through a set of equations. In the general case, analytical solution cannot be found, hence the use of numerical resolution methods. As a consequence, the discretization of the volume and the time range are required to compute approximations of the solution. Among all the numerical techniques available, one can divide them in two main categories. Mesh-based techniques features connectivity information between the interpolation points whereas meshless methods rely on a set of uncorrelated points. The abrasion process simulation includes large deformations so that a regeneration algorithm is often needed to handle element distortion. Concerning meshless methods, the particle distribution used to interpolate vector fields inside the specimen allows to take into account any amount of deformation whether small or large. That's why particle-based methods are a suitable choice for wear simulations. Finite Volume Particle Method (*FVPM*) is a meshless method which includes many of the attractive features of both particle methods, such as SPH, and conventional mesh-based Finite Volume Methods (FVM) [10]. In *FVPM*, the Sheppard function is used as the interpolating

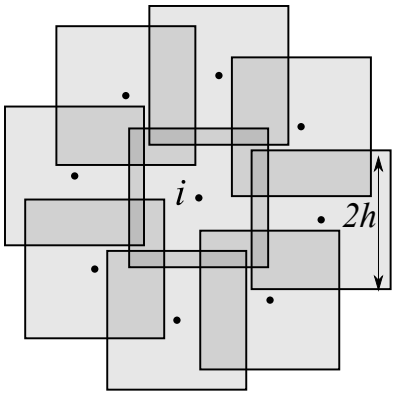

Figure 1: rectangular support kernels

function defined by equations 3 and 4:

$$W_i = \begin{cases} 1 & \|\mathbf{x} - \mathbf{x}_i\|_\infty \leq h_i \\ 0 & \|\mathbf{x} - \mathbf{x}_i\|_\infty > h_i \end{cases} \tag{3}$$

$$\psi_i = \frac{W_i(\mathbf{x})}{\sum\limits_k W_k(\mathbf{x})} \tag{4}$$

$$\mathbf{U} = \sum_i \psi_i \mathbf{u}_i \tag{5}$$

Any spatial field can be interpolated from the spatial scheme composed of overlapping particles, as shown in Figure 1. The kernel function W_i defined by equation 3 allows to take into account the neighbor particles within a defined domain size h_i. The equation 4, which sets the Shepard value ψ_i for a given point, consists in a normalization of the kernel over all the considered particles. Equation 5 gives the value U of the interest quantity as the summation over all the neighboring particles. This principle allows to retrieve the value at any given point in between particles. Since no connectivity information is embedded in the particle cloud, an additional cost is driven by the need to retrieve closest neighbors. Nevertheless spatial hashing algorithms allow to reduce the addressed complexity. The interpolation of the derivatives is carried out with the same spatial discretization.

$$\rho \frac{d\mathbf{C}}{dt} = \nabla \,.\, \sigma + \rho \mathbf{g} + \mathbf{f}_c \tag{6}$$

The equation 6 accounts for the internal equilibrium that structures the solid in question and represents a local application of the fundamental principle of dynamics. The velocity field of the solid is denoted by $\mathbf{C}$ and σ represents the stress tensor. The solid is eventually subjected to gravity $\mathbf{g}$ and external forces $\mathbf{f}_c$. Solving this equation requires the evaluation of the divergence of constraints $\nabla \,.\, \sigma$. The speed of sound is given by the material's Young's modulus, E, and Poisson's ratio, ν, according to:

$$v = \sqrt{\frac{E}{3\rho_0(1-2\nu)}} \tag{7}$$

The *FVPM* method is based on calculating the stress divergence through the flow that passes through the common surface between two adjacent interpolation zones (Eq. 8).

$$\int_{\Omega_i} \nabla \,.\, \sigma = \oint_{S_i} \sigma \,.\, d\mathbf{S} = \oint_{S_i} \mathbf{n} \,.\, \sigma \,.\, dS = \sum_j (\mathbf{\Gamma}_{ij} - \mathbf{\Gamma}_{ji}).\sigma_{ij} \tag{8}$$

$$\mathbf{\Gamma}_{ij} = -\sum_{l=1}^{m} \left(\frac{\Delta \mathbf{S}_l}{\delta_l^+ \delta_l^-} \right) \tag{9}$$

The integral of the divergence of constraints in the volume Ω_i is calculated using the flow-divergence theorem and solved numerically in equation 9 based on neighboring volumes as shown in Figure 2. The variables δ_+ and δ_- denote the kernel summation outside and inside the particle number i. The Figure 2 depicts the calculation of interaction vector $\mathbf{\Gamma}_{ij}$ between particle i and j. The area is partitioned into surfaces of constant δ_+ and δ_- and the intersection border is divided into 4 segments. Each segment corresponds to one term in the summation of equation 9. The superposition of rectangular supports is necessary to calculate the interactions between the particles. The choice of this geometry was made in order to accurately calculate the contact surfaces between the rectangular supports. More details on the implementation of this method can be found in [11].

In order to link strain and stress, the Johnson Cook model is implemented. This model includes a non-linear hardening coefficient n and the effect of strain rate $\dot{\varepsilon_p}$ and temperature T_*.

$$\sigma = \left[A + B\varepsilon_p^n \right] \left[1 + C ln \left(\frac{\dot{\varepsilon_p}}{\dot{\varepsilon_0}} \right) \right] \left[1 - T_*^m \right] \tag{10}$$

The failure of the material is modeled by the removal of particles whose plastic strain reaches a certain value ε_f. This value is a function of the strain rate $\dot{\varepsilon_p}$, the pressure p relative to the von Mises stress σ_v and the temperature T_*. The parametrization of this model relies on five material constants D_i.

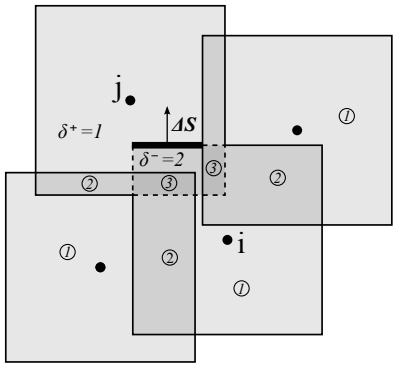

Figure 2: Interactions between particles i and j [11]

$$\varepsilon_f = \left[D_1 + D_2 \, exp(D3 \frac{p}{\sigma_v}) \right] \left[1 + D_4 \left(\frac{\dot{\varepsilon_p}}{\dot{\varepsilon_0}} \right) \right] \left[1 + D_5 \, T_* \right] \tag{11}$$

In *FVPM*, like in SPH, computational nodes usually move with the material velocity, which is compatible with the Lagrangian form of the equation of motion. This enables the method to handle moving interface problems without issues of mesh deformation or tangling. Contrary to mesh-based methods, whose core functions rely on generating a rigidity matrix to be inverted, working with particles as interpolation points implies to compute internal forces exerted on each particle at each time step. The forces are correlated to accelerations which are integrated as time passes from one step to another. The propagation of acoustics waves in the specimen is part of the outcomes of the simulation. Thus, using this force based framework raises numerical instabilities against the chosen time step. The plasticity simulation is based on radial return stress evaluation.

$$CFL = \frac{v \delta t}{\delta x} \tag{12}$$

The *CFL* condition given in equation 12 ensures that the numerical integration scheme is stable. It is depends on the characteristic speed v in the material, the value of time steps δt and the particle spacing δx. *CFL* number is comprised between 0 and 1 which, in turn, bounds the time step to keep the simulation stable. A refinement of the particle spacing δ_x will not only lead to an increase in the number of particles but also to a reduction in the time step.

The presented article is based on a *FVPM* implementation developed by [12] which is named *SPHEROS*. This simulation code features several solvers emulating fluid or solid behavior and relies on the *open MPI* [13] message passing interface for

parallel computations on clusters. The elasto-plastic deformations induced by a rigid spherical particle over the specimen surface have been evaluated to complete the erosion simulations resulting from the impact of silt particles on a surface [11]. Residual stress repartition have been found coherent with [14]. The main difference between erosion and abrasion lies in the amount of plastic strain reach by the specimen, and which is much more important concerning abrasion.

3. Scratching test case

The scratching test consists in damaging a solid under the motion of an indenter. The indenter moves tangentially to the surface under a normal load which results in the creation of a scratch. The geometry of the groove associated with the required efforts characterize the ability of the solid to resist to local plastic deformations. The scratching simulation has been done on copper, since this material characteristics have been widely studied in the literature. The associated material properties and Johnson Cook material parameters are listed in tables 1, 2 and 3.

Table 1: Material properties for copper

Material property	Value	Unit
Density, ρ	8960	$[kg.m^{-3}]$
Young's modulus, E	124	$[GPa]$
Poisson's ratio, ν	0.34	[-]

Table 2: Johnson-Cook parameters for copper

Parameter name	Value	Unit
Initial yield stress, A	90	$[MPa]$
Hardening coefficient, B	292	$[MPa]$
Hardening exponent n	0.31	[-]

Table 3: Johnson-Cook damage parameters for copper

Parameter name	Value	Unit
D_1	0.54	[-]
D_2	4.89	[-]
D_3	-3.03	[-]
D_4	0.014	[-]
D_5	1.12	[-]

The specimen is composed of overlapping particles as shown in Figure 3. The repartition of particles is generated as an assembly of two sphere quarters and a half cylinder. The spheres are located at the edges and the cylinder represents the core of the specimen. This repartition consists in an assembly of several hulls whose distance to the center line of the specimen is the same and whose particle diameter is constant. An example of one hull is given in Figure 4. This repartition is suitable to generate regular variation of particles radius in the specimen. In this respect, the particles are always surrounded by others with

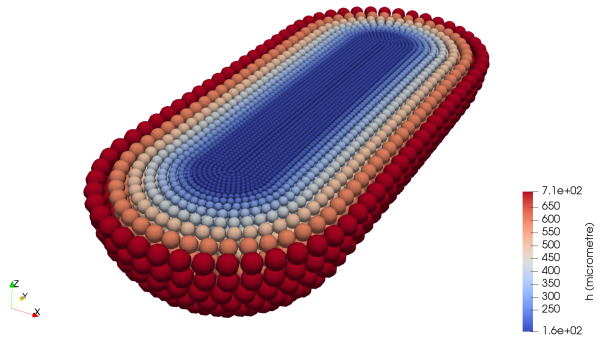

Figure 3: Specimen particle repartition

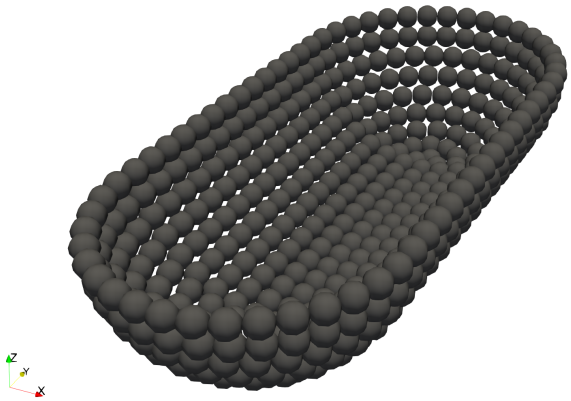

Figure 4: Fixed particles for boundary condition

a similar size. This avoid the instabilities generated in the interface due to large variation of particle size in the same area. The spacing length is refined in the areas of interest to balance relevance against computing time while the largest particles aim at extended the size of the simulation without penalizing computational complexity. The finest particles have a diameter 15 times smaller than the indenter in the presented test case.

The indenter is modeled by a single spherical particle. The indenter size in this simulation has a 400 μm diameter. The interaction between the specimen and the spherical particle modeling the indenter consists in a penalty force directed from the center of the indenter toward each of the particle in contact. Although the Coulomb model for friction is available in the code, the friction not been taken into account to stay coherent with [7]. In the simulation, the indenter speed is 100 m.s^{-1} whereas experimental speed is 10 mm.s^{-1}. The high speed chosen here does not reflect reality, but reduces the simulation time [15]. The C coefficient of the equation 10 has been set to zero so that the indenter velocity has no influence on the specimen behavior. This allows to use a relatively high speed of scratching. This choice has been imposed by the fact that the *FVPM* model simulates the material strain and stress based on a dynamic res-

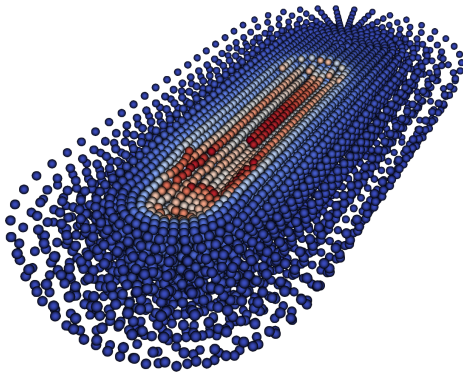

Figure 5: Simulation result for h_s 60 μm

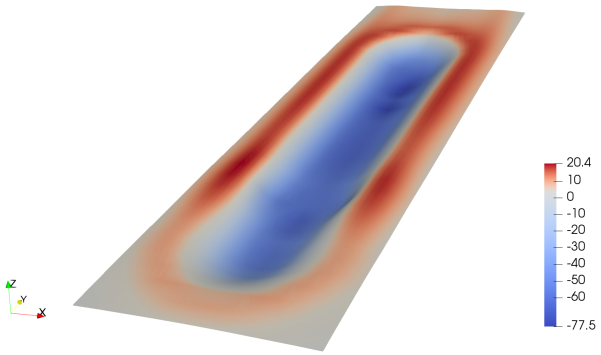

Figure 6: Extracted topography heights [μm]

olution of the equations. The kinematics of the indenter consists in a vertical descent until the chosen penetration depth is reached. Then the indenter slides tangentially to the surface over a distance defined 10 times longer than its radius.

The simulations have been run in a computational cluster. The main characteristics of the test case are listed in table 4.

Table 4: Simulation characteristics

Number of cores	64
Number of particles	21143
Simulation time	5 h 28 min

4. Results and discussion

Several simulations have been run with different penetration depth h_s from 5 μm to 60 μm. A screen shot of the simulation is displayed in Figure 5. In Figure 6 the surface has been extracted from the points cloud using a level set of an implicit function. As shown in Figure 6 bulges are present at the side of the indentation.

The evolution of the normal load L and tangential effort F has been plotted against scratching distance D in Figure 7. The first part of the curve corresponds to the indentation. At this point, normal effort is maximum and tangential effort is still null. Then, as the indenter begins to slide over the surface, tangential resistance is opposed to the motion and leads to a stationary state. Oscillations are observed from these curves and are due to the periodical removal of damage particles during the simulation.

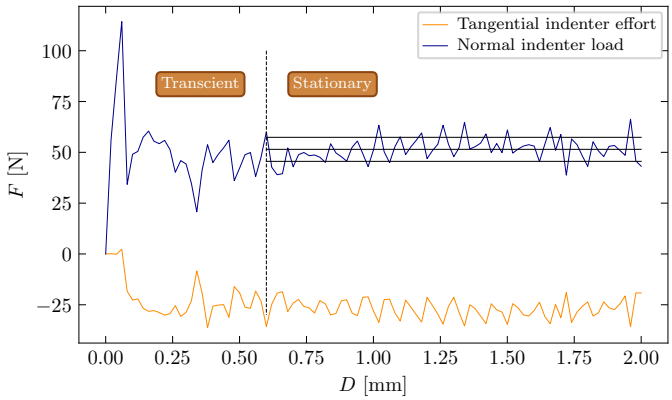

Figure 7: Scratching efforts for a 60 μm depth

For each indentation depth, the corresponding normal load L and tangential effort T have been collected in the simulated data and plotted in Figures 8 and 9. In addition, the numerical results obtained have been compared with the article of Leroch [7] in these two figures. Orders of magnitude of the proposed simulations are consistent with the literature. Normal load simulated with the *FVPM* model tends to over estimate the real value whereas tangential efforts are coherent. For small indentation depth, the normal load is higher than both experimental and simulated literature results. For medium loads the values fit the literature data. While the depth reaches the highest values, the uncertainty increases because of the high damages generated in the specimen which leads to particles being periodically removed. The fact that friction coefficient has not been taken into account may explain the tangential effort tendency to be under the other values. The particle distribution used with the *FVPM* model, which is coarser than [7], may have an influence in the over estimation of normal load.

5. Conclusion

The elasto-plastic *FVPM* model implemented in *SPHEROS* have been assessed for the problem of scratching a specimen under the tangential motion of an indenter. The chosen simulations conditions aimed at replicating the main raw interactions encountered during the abrasion process.

The simulation kinematics have been imposed and the efforts have been observed afterward. Various penetration depth have been tested. The topography is coherent with experimen-

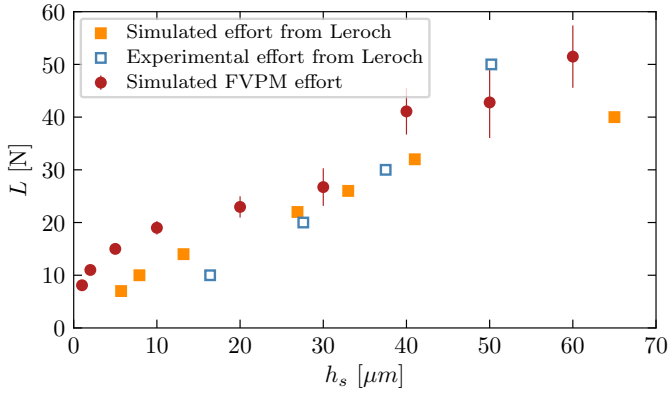

Figure 8: Normal load exerted on the indenter

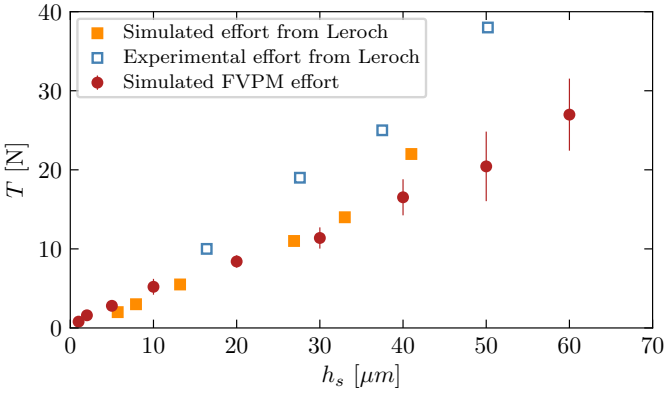

Figure 9: Tangential load exerted on the indenter

tal observations found in literature. *FVPM* appears to be an interesting alternative to molecular dynamic model or SPH algorithms. Nevertheless numerical instabilities have been encountered while large plastic strain was reached. The plastic simulation algorithm based on radial return stress evaluation may not to be sufficiently stable for large deformations.

This issue need to be considered before investigating the implementation of a several particles grinding process. The simulation framework is suitable for taking into account abrasive tool wear during the process. An increased computing time is expected against the problem complexity, which will need to be addressed.

The primitive geometry for the indenter could be model by an elasto-plastic model in order to simulate abrasive wear which is a common problem while industrializing mechanical part.

References

[1] K. Z. Gahr, Preface, in: Microstructure and Wear of Materials, Elsevier, 1987, pp. v–vi (1987).

[2] H. Tönshoff, J. Peters, I. Inasaki, T. Paul, Modelling and simulation of grinding processes, CIRP Annals 41 (2) (1992) 677–688 (1992).

[3] E. Brinksmeier, J. Aurich, E. Govekar, C. Heinzel, H.-W. Hoffmeister, F. Klocke, J. Peters, R. Rentsch, D. Stephenson, E. Uhlmann, K. Weinert, M. Wittmann, Advances in modeling and simulation of grinding processes, CIRP Annals 55 (2) (2006) 667–696 (2006).

[4] F. Klocke, O. Dambon, B. Behrens, Analysis of defect mechanisms in polishing of tool steels, Production Engineering 5 (5) (2011) 475–483 (feb 2011).

[5] X. Chen, W. B. Rowe, Analysis and simulation of the grinding process. part II: Mechanics of grinding, International Journal of Machine Tools and Manufacture 36 (8) (1996) 883–896 (aug 1996).

[6] F. W. Preston, The theory and design of plate glass polishing machine, J. soc. Glass technol 11 (1927) 214–256 (1927).

[7] S. Leroch, M. Varga, S. Eder, A. Vernes, M. R. Ripoll, G. Ganzenmüller, Smooth particle hydrodynamics simulation of damage induced by a spherical indenter scratching a viscoplastic material, International Journal of Solids and Structures 81 (2016) 188–202 (mar 2016).

[8] M. Takaffoli, M. Papini, Finite element analysis of single impacts of angular particles on ductile targets, Wear 267 (1-4) (2009) 144–151 (jun 2009).

[9] M. Takaffoli, M. Papini, Material deformation and removal due to single particle impacts on ductile materials using smoothed particle hydrodynamics, Wear 274-275 (2012) 50–59 (jan 2012).

[10] R. J. LeVeque, Finite volume methods for hyperbolic problems 298 (2002) 80–107 (2002).

[11] E. Jahanbakhsh, C. Vessaz, F. Avellan, Finite Volume Particle Method for 3-D Elasto-Plastic Solid Simulation, in: Proceedings of the 9th international SPHERIC workshop, 2014 (2014).

[12] E. Jahanbakhsh, Simulation of silt erosion using particle-based methods (2014).

[13] E. Gabriel, G. E. Fagg, G. Bosilca, T. Angskun, J. J. Dongarra, J. M. Squyres, V. Sahay, P. Kambadur, B. Barrett, A. Lumsdaine, R. H. Castain, D. J. Daniel, R. L. Graham, T. S. Woodall, Open MPI: Goals, concept, and design of a next generation MPI implementation, in: Proceedings, 11th European PVM/MPI Users' Group Meeting, Budapest, Hungary, 2004, pp. 97–104 (September 2004).

[14] S. Meguid, G. Shagal, J. Stranart, J. Daly, Three-dimensional dynamic finite element analysis of shot-peening induced residual stresses, Finite Elements in Analysis and Design 31 (3) (1999) 179–191 (jan 1999).

[15] F. Ducobu, E. Rivière-Lorphèvre, E. Filippi, On the introduction of adaptive mass scaling in a finite element model of ti6al4v orthogonal cutting, Simulation Modelling Practice and Theory 53 (2015) 1–14 (apr 2015).